WATER RESOURCES RESEARCH, VOL. 49, 4054–4070, doi:10.1002/wrcr.20327, 2013

Palaeohydrogeological insights from natural tracer profiles in aquitard porewater, Great Artesian Basin, Australia

Glenn A. Harrington,[1] W. Payton Gardner,[1,2] Brian D. Smerdon,[1] and M. Jim Hendry[3]

Received 31 July 2012; revised 1 May 2013; accepted 23 May 2013; published 8 July 2013.

[1] The value of using environmental tracer profiles in aquitards to quantify fluid flux and to reveal information about palaeohydrology is largely unknown for parts of the world that were not glaciated during the Cenozoic. We present deep, continuous vertical profiles of aquitard pore water chloride concentration and $\delta^2H/\delta^{18}O$ composition from the western margin of the Great Artesian Basin, Australia, where upward leakage is the dominant groundwater discharge mechanism. At the deeper of the two sites studied, the Cl^- and δ^2H profiles exhibit a distinctive S-shape, which we interpret as a shift in the upper concentration boundary condition over time. Numerical simulations are used to support an hypothesis that the shallow phreatic aquifer was more saline and more enriched in δ^2H compared to current conditions prior to ~120 ka, followed by an extended freshening phase from ~120 to 20 ka, then a saline phase similar to current conditions for the last ~20 ka. These timeframes correspond favorably with results of previous studies into the palaeohydrology of nearby playa Lake Eyre. At the shallower site, the tracer profiles decrease exponentially with depth. We explore several models for the evolution of these profiles and adopt one of long-term salt input at ground surface. At both sites, tracer concentrations for groundwater sampled from the underlying artesian aquifer provide conclusive evidence that recharge occurred within the last 10–20 ka. Chloride was a more useful tracer than δ^2H in this study, primarily due to lack of recent glaciation in central Australia to provide a dynamic δ^2H tracer signal.

Citation: Harrington, G. A., W. P. Gardner, B. D. Smerdon, and M. J. Hendry (2013), Palaeohydrogeological insights from natural tracer profiles in aquitard porewater, Great Artesian Basin, Australia, *Water Resour. Res.*, *49*, 4054–4070, doi:10.1002/wrcr.20327.

1. Introduction

[2] Aquitards can have a profound impact on groundwater flow and solute transport in adjacent aquifers. These low permeability layers maintain confined aquifer hydraulic conditions and impede interaquifer leakage of water and contaminants. They often contain large reservoirs of high salinity pore fluid that leaks over very long time scales to contiguous aquifers. Despite these factors, and the increasing global demand for below-ground hazardous waste disposal in low-permeability media, there are still fewer studies of aquitards than aquifers.

[3] One of the most promising avenues of aquitard research over the last few decades is the application of natural tracer profiles to estimate formation-scale fluid flux [*Desaulniers et al*., 1981; *Sanford and Wood*, 1995; *Hendry and Wassenaar*, 1999] and to shed light on long-term climatic and geologic conditions [*Neuzil*, 1993; *Birks et al*., 2000; *Hendry and Woodbury*, 2007; *Mazurek et al*., 2011; *Hendry et al*., 2011]. However, because of the high cost of obtaining such profiles, most previous studies have only focused on one or two tracers and/or aquitard core sites. Hence there is a need for increased research on the application of multiple tracers to gain regional insights into water fluxes and solute transport. Available literature suggests that profiles of the stable H/O isotopes of water provide the most conclusive information about long-term climatic and geologic shifts, although this is largely due to the importance of glaciation in the regions studied—the western plains of North America and central Europe. Other tracers that can be particularly useful for constraining estimates of aquitard hydraulic conductivity (K), and thus fluid flux, include halogens and other ions [*Hendry and Wassenaar*, 2000; *Hendry et al*., 2000], radiocarbon [*Wassenaar and Hendry*, 2000], and helium-4 [*Osenbrück et al*., 1998; *Hendry et al*., 2005; *Gardner et al*., 2012].

[4] The application of multiple tracers to aquitard studies has previously been undertaken in the northern hemisphere, where glaciation during the Tertiary and/or Quaternary provided a transient input function. In contrast, very few studies have been undertaken in the southern hemisphere. The only noteworthy exception is the Otway Basin in southeastern Australia [*Love et al*., 1996; *Harrington et al*.,

[1]CSIRO Water for a Healthy Country National Research Flagship, CSIRO Land and Water, Waite Campus, Private Bag 2 Glen Osmond SA, 5064, Australia.
[2]Sandia National Laboratories, Albuquerque, New Mexico, USA.
[3]Department of Geological Sciences, University of Saskatchewan, 114 Science Place Saskatoon SK, S7N5E2, Canada.

Corresponding author: Glenn A Harrington, CSIRO, Land & Water, Waite Road, Urrbrae, SA 5064l, Australia. (Glenn.Harrington@csiro.au)

0043-1397/13/10.1002/wrcr.20327

2001] although the aquitard in this case is very thin (i.e., less than 50 m). Hence there is a need to test the application of environmental tracers to aquitard systems in nonglaciated regions as a means of determining long-term climatic and geologic conditions and constraining estimates of fluid flux.

[5] The Great Artesian Basin (GAB) is one of the largest groundwater systems in the world, covering more than 1.7 million square kilometers or approximately one-fifth of the Australian continent. Groundwater resources from the GAB sustain pastoral and mining industries, as well as domestic and municipal demands, and many important wetland habitats across remote, extensive and generally arid parts of the continent. Despite the importance of this resource, the bulk of research to date has focused on either groundwater recharge and flow within the main Jurassic-Cretaceous sandstone aquifer [*Habermehl*, 1980; *Bentley et al*., 1986; *Mazor*, 1995; *Bethke et al*., 1999; *Love et al*., 2000; *Kellet et al*., 2003; *Habermehl et al*., 2009] or quantifying discharge via springs [*Williams and Holmes*, 1978; *White and Lewis*, 2011]. Only two studies have attempted to measure diffuse discharge from the GAB via upward leakage through the regional aquitard. Using shallow soil-water chloride and deuterium profiles, *Woods et al*. [1990] estimated evaporation rates of 0.5–7 mm a^{-1} in the southwestern margin of the GAB, which they assumed represented diffuse upward leakage. Similar research by *Costelloe et al*. [2008] also used soil-water chloride profiles, in conjunction with eddy correlation and microlysimeters, to derive evaporation rates from the soil zone. In practice, however, the water balance of shallow phreatic aquifers overlying the GAB will have a component of recharge from episodic rainfall and flooding [*Cendón et al*., 2010], so the fluxes derived from these earlier studies should be considered as uppermost limits of diffuse discharge from the GAB. No previous studies have attempted to measure diffuse leakage through the aquitard that overlies the GAB.

[6] The objective of this paper is to provide greater understanding and awareness of the value of using multiple environmental tracers to study leakage through aquitards. In doing so, we specifically test the application of chloride and stable H/O isotope profiles for the first time in the southern hemisphere where glaciation has not occurred. Through measurement and modeling of two sets of profiles separated by about 25 km, we obtain valuable insights to the long-term hydrological history of the southwest margin of the GAB, and the spatial variability of vertical fluid flux through the aquitard.

2. Modeling Concepts and Equations

[7] The transport of a conservative tracer in a porous medium with uniform one-dimensional flow in the vertical direction is governed by

$$\frac{\partial \eta_e C}{\partial t} = \frac{\partial}{\partial z}\left(\eta_e D \frac{\partial C}{\partial z}\right) - \frac{\partial}{\partial z}(v_z \eta_e C), \tag{1}$$

where η_e is the effective porosity, C is the concentration, t is the time, D is the dispersion coefficient, v_z and z are linear pore water velocity and distance in the vertical direction, respectively. Effective porosity, often termed "solute-accessible" porosity, is less than the total porosity (η) because not all pore spaces in a medium are available for solute transport. This is particularly the case for anions, due to the formation of a double-diffusive layer of repulsion on the surface of negatively charged clay minerals. Hence, values of η_e for anion transport are generally lower than those for cations or uncharged species (e.g., H_2O, HDO, and HTO), although η_e approaches η as ionic strength increases [*Van Loon et al*., 2007].

[8] The dispersion coefficient D in equation (1) can be expressed as

$$D = \alpha_v v_z + D_p, \tag{2}$$

where α_v is dispersivity in the vertical direction (z), and D_p is the "pore-water" diffusion coefficient, also in the vertical direction. This expression neglects the nondiagonal terms of the dispersion tensor, which is acceptable for the current study as we are only considering flow and transport in the vertical direction. Substituting equation (2) into (1) yields a dispersion and diffusion term, and the latter can be defined with

$$D_e = \eta_e D_p, \tag{3}$$

where D_e is known as the "effective" diffusion coefficient. In low-permeability media, when advective flux is very small (i.e., $v_z << D_e/\eta_e\alpha_v$), estimating D_e becomes important for simulating the diffusive transport of solutes. An underestimation of D_e will lead to overestimation of the timeframe for evolution of the tracer profile, and vice versa, although it will not change the ultimate shape of the diffusion profile.

[9] Many studies have determined D_e for specific solutes using either laboratory diffusion-cell experiments [*Novakowski and van der Kamp*, 1996; *Hendry et al*., 2000; *Mazurek et al*., 2011] or field tracer studies [*Barbour et al*., 2012]. Where this is not possible, theoretical expressions such as the following can be applied to estimate D_e (e.g., *Freeze and Cherry* [1979]; *Fetter* [1993]; *Ingebritsen et al*. [2006]):

$$D_e = \omega D_0, \tag{4}$$

where ω is a constant of proportionality with a value less than one (typically 0.01–0.5; *Freeze and Cherry*, 1979], and D_0 is the free water diffusion coefficient. A number of different mathematical expressions for ω exist in the literature, all of which are functions of formation tortuosity (τ), constrictivity (δ), and/or porosity (η or η_e). For example (after *Boving and Grathwohl* [2001]),

$$D_e = \eta_e \tau \delta D_0. \tag{5}$$

[10] The constrictivity ($\delta \leq 1$) is a dimensionless parameter that can be neglected when the size of the pores is greater than 1 nm [*Grathwohl*, 1998]. Various equations also exist for tortuosity, but in this case,

$$\tau = \left(\frac{l}{l_e}\right)^2 \tag{6}$$

where l is the direct, linear distance of travel in the medium, and l_e is the effective path length for solute transport through the pores; hence $\tau < 1$.

[11] As an alternative to equation (5), D_e can be expressed in the form of Archie's Law

$$D_e = \eta^m D_0, \tag{7}$$

where m is an empirical exponent. *Boving and Grathwohl* [2001] report literature values for m ranging from 1.3 to 2, and present iodide tracer experimental results where m=2.2 for sandstone and limestone samples. Similarly, *Mazurek et al*. [2011] report values of 2–3 for HTO and 2–2.5 for anions, based on laboratory measurements of D_e and η for nine clay-rich aquitard sites in central Europe.

[12] In addition to porosity and ionic strength, temperature can have significant effect on diffusion coefficients. *Van Loon et al*. [2005] demonstrated how the effect of temperature on the diffusion coefficient can be explained by an Arrhenius equation, in which the activation energies (E_A) for $^{22}Na^+$, $^{36}Cl^-$, and HTO can all be assumed as being equal to 20 ± 1 kJ·mol^{-1}, so that

$$D_e = \eta_e \tau \delta A e^{-\frac{E_A}{RT}}, \tag{8}$$

where A is an empirical Arrhenius parameter [L^{2}T^{-1}], R is Boltzmann's constant (8.31451 J·mol^{-1}·K^{-1}), and T is temperature (K). It follows from equation (8) that the ratio of effective diffusion coefficients for a given solute and porous medium at temperatures T_2 and T_1 can be expressed as

$$\frac{D_{e,T_2}}{D_{e,T_1}} = e^{\frac{E_A}{R}\left(\frac{1}{T_1}-\frac{1}{T_2}\right)} \tag{9}$$

[13] Thus, for Na^+, Cl^-, and HTO (and by inference HDO) the difference between effective diffusion coefficients at 20°C and 40°C is a factor of approximately 1.7.

3. Materials and Methods

3.1. Site Description

[14] Two deep, continuous, aquitard cores were drilled in the southwest margin of the GAB during June–July 2010. This part of the GAB is the main discharge area for groundwater flow from the north-western and eastern recharge areas (Figure 1); groundwater ages are generally in the range $10^5 - 10^6$ years [*Torgerson and Clarke*, 1985; *Love et al*., 2000]. The region is arid with mean annual areal potential evapotranspiration ~1300 mm a^{-1} far exceeding mean annual rainfall <200 mm a^{-1}.

[15] The locations of the two core sites were selected to represent different aquitard stratigraphy and vertical hydraulic gradient, and were located within 100 m of existing wells completed in the confined Jurassic-Cretaceous (J-K) aquifer (Figure 1). The latter was necessary to provide depth control so that drilling did not penetrate the underlying artesian aquifer, as well as to enable head measurements and water samples from the J-K aquifer for chemical and isotopic analysis. The cored hole at Birthday Bore (BB2) was drilled to a total depth of 102 m below ground surface (BGS; cf. top of the J-K aquifer at ~110 m BGS), while the cored hole at Nancy's Bore (NB2) was drilled to 290 m BGS (cf. top of the J-K aquifer at ~324 m BGS). The drill fluids were spiked with 99% deuterium oxide (i.e., liquid ^2H_2O) to provide a tracer for core contamination; this was achieved by adding 250 mL of deuterium oxide to every 15,000 L refill of the water truck. The source water for the drill fluids was the existing well completed in the J-K aquifer at each site. A single piezometer was also installed at the time of drilling in the shallow phreatic aquifer at each site (see Table 1 for completion depths).

3.2. Local Hydrogeology

[16] At BB2 approximately 20 m of unconsolidated Quaternary sediment overlies 90 m of Cretaceous Bulldog Shale and the J-K sandstone aquifer (Figure 2). The Bulldog Shale is best described as a dark grey, bioturbated, and fossiliferous marine mudstone, with pale grey micaceous silt to very fine sand intervals [*Krieg*, 1995]. This description is consistent with observations of the cored section of Bulldog Shale recovered from both sites. The measured porosity of the Bulldog Shale, which is presented later, is also more typical of values for shallow buried mudstones (e.g., see *Yang and Aplin* [2010]) than shales.

[17] At NB2, approximately 18 m of unconsolidated Quaternary sediment overlies 306 m of Cretaceous aquitard comprising, from top to bottom, approximately 102 m of Oodnadatta Formation (a fine-grained sandy siltstone), 31 m of Coorikiana Sandstone and 172 m of Bulldog Shale.

[18] Water levels in the shallow piezometers at BB2 and NB2 were 3.5 m BGS and 12.0 m BGS (respectively) while shut-in pressures for the J-K aquifer at each site were 16.1 m and 25.2 m above ground surface (respectively) (Table 2). These heads reveal an upward hydraulic gradient of 0.150 at BB2 and 0.117 at NB2. Further details of aquitard lithology and hydraulic properties are provided in *Smerdon et al*. [2012].

3.3. Sampling and Analytical Procedures

[19] Aquitard cores were recovered in 3 m lengths and sampled for a suite of physical, chemical, and dissolved gas analyses at varying spatial resolution. Samples for major ion analysis were taken at approximately 5 m intervals, yielding 15 samples from BB2 (22.1–102.1 m BGS) and 49 samples from NB2 (36.3–289.6 m BGS) (Table 1). Samples for δ^2H and $\delta^{18}O$ analyses were also taken at approximately 5 m intervals, yielding 16 samples from BB2 (22.0–102.0 m BGS) and 48 samples from NB2 (35.9–289.8 m BGS) (Table 1). For both major ion and stable isotope samples, the outer 1–2 mm of core was shaved and discarded to avoid any potential contamination by drilling fluid. Every piece of core was vacuum sealed in Food Saver® bags then placed in large (2 L) ziplock bags and stored in insulated coolers.

[20] Major ion samples were analyzed for chloride concentration, and later bromide concentration (selected samples), by liquid ion chromatography on 1:3 paste extracts using double-deionized water at CSIRO Land and Water, Adelaide.

[21] The stable isotope samples were air freighted to Canada soon after drilling and arrived at the University of Saskatchewan in July 2010. Upon arrival, the samples were transferred from the Food Saver bags into medium (945

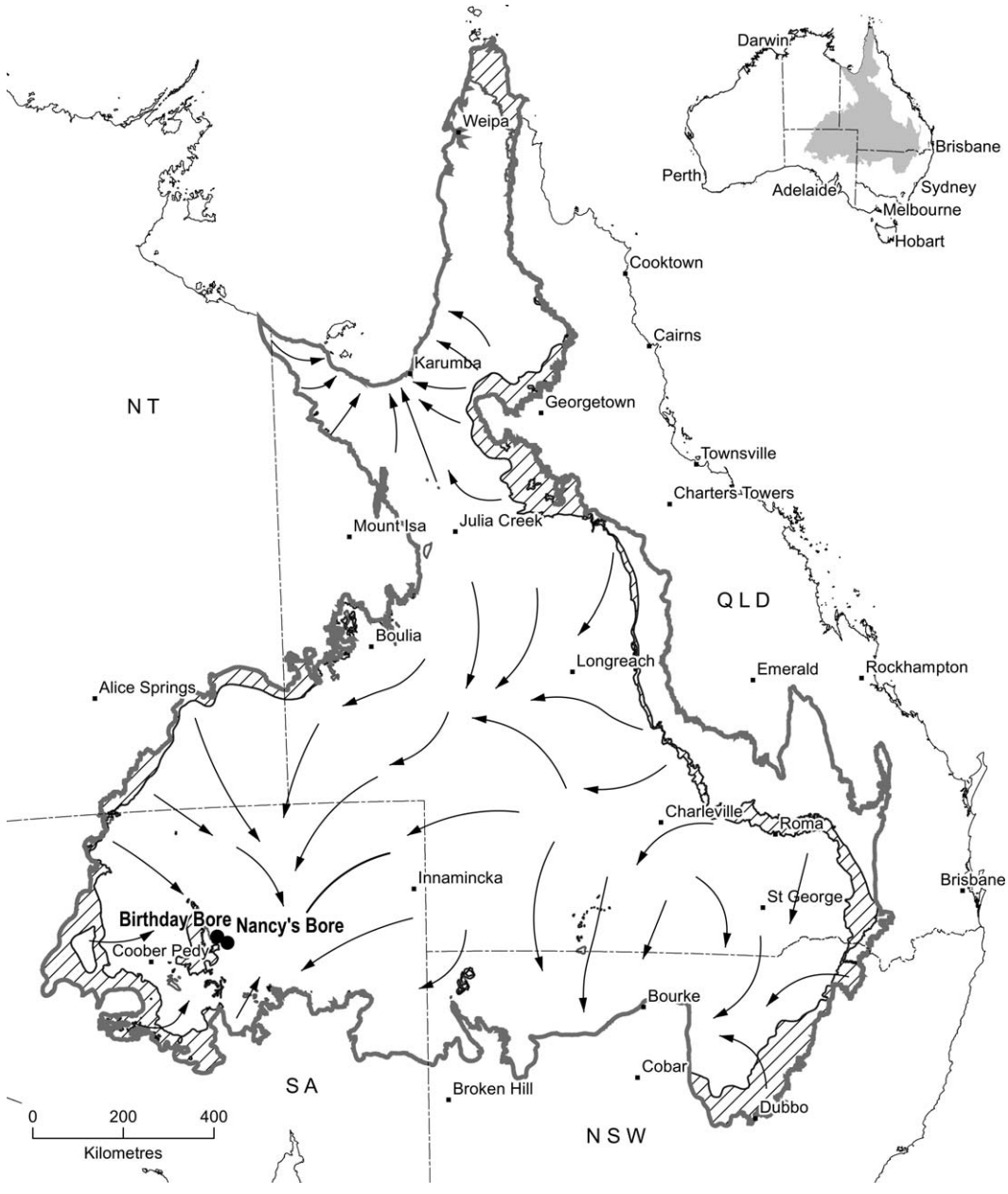

Figure 1. Location of Birthday Bore (BB2) and Nancy's Bore (NB2) study sites at the south-western margin of the GAB, Australia. Arrows represent inferred groundwater flow lines and hatched areas represent recharge beds for the main J-K aquifer.

mL) ziplock bags, then doubled bagged in a large (2 L) ziplock bag, and stored in coolers until they were run for δ^2H and δ^{18}O analyses in September 2010.

[22] A small portion of core (<2 cm) was taken from the stable isotope samples for determination of gravimetric water content (GWC) by drying at 90°C. Bulk density and specific gravity were also measured using standard methods (*ASTM*, 2009, 2010). This enabled Cl^- concentrations measured on paste extracts to be converted into porewater concentrations. The GWC and bulk density data also enabled computation of total porosity (n = 48 for NB2, n = 16 for BB2).

[23] All core samples were run for δ^2H and δ^{18}O on a Piccarro L1102-i in September 2010 using the vapor equilibration method outlined in *Wassenaar et al*. [2008]. During the analysis, no methane was detected using the Picarro L1102-i. Three standards were used while running the samples, Bir (−178 δ^2H, −23 δ^{18}O), Sk-T (−130 δ^2H, −16 δ^{18}O), and HdD (+72 δ^2H, −16 δ^{18}O). Multiple reruns were performed on the NB2 and BB2 core samples: NB2 samples were rerun two or three times while BB2 samples produced more consistent results and were only rerun once. The mean and standard deviation from all δ^2H and δ^{18}O analyses at each depth are listed in Table 1.

[24] Soon after drilling, representative groundwater samples were collected from the existing J-K aquifer wells at each site, and the new piezometer at BB2. Unfortunately, samples could not be obtained from the shallow

Table 1. Groundwater Chemistry and Isotopic Data From the Phreatic Aquifer, Aquitard Pore Water, and J-K Aquifer at Nancy's Bore and Birthday Bore

Sample ID	Major ion sample depth (m BGS)	Cl (mg L^{-1})	Br (mg L^{-1})	Cl/Br (molar)	Stable isotope sample depth (m BGS)	$\delta^{2}H$ (‰ VSMOW)		$\delta^{18}O$ (‰ VSMOW)		Carbon-14 (pmC)	
						μ	1σ	μ	1σ	μ	1σ
NB2 piezometer (phreatic)											
	36.3	5355			35.90	−23.5	4.1	−3.42	0.72		
	39.2	4568	4.8	2144	39.20	−23.6	1.3	−1.46	2.17		
	43.2	4810			42.10	−22.9	3.8	−2.67	1.18		
	50.1	4499	5.5	1844	49.90	−23.4	1.7	−2.75	0.57		
	53.9	3877			53.60	−23.4	2.1	−3.69	0.35		
	61.1	4087	5.3	1726	59.90	−26.1	0.7	−3.20	1.37		
	63.5	3883			63.32	−21.0	4.5	−2.80	1.17		
	70.6	3566			70.50	−27.8	2.0	−3.66	0.76		
	75.2	4170			75.25	−20.5	1.4	−2.67	1.46		
	81.2	3840			81.05	−26.9	7.3	−3.24	1.47		
	85.7	4053			85.85	−32.9	5.5	−2.71	2.11		
	90.7	3501			90.55	−30.0	4.8	−2.66	1.55		
	96.1	4445			95.35	−29.5	4.3	−3.15	2.08		
	101.4	3834			101.26	−30.6	0.4	−3.96	1.57		
	107.4	5369			107.10	−26.6	3.1	−3.48	1.12		
	113.5	4864			113.30	−23.1	2.1	−3.50	2.12		
	119.4	5003	4.2	2704	119.30	−31.3	5.6	−2.53	2.07		
	119.8	2818			125.10	−25.6	4.7	−3.13	1.30		
	125.4	4465			130.00	−21.0	0.6	−3.05	0.83		
	130.0	4741	4.9	2201	134.90	−21.6	1.2	−3.24	1.67		
	135.2	5348			140.10	−23.5	0.8	−2.91	1.16		
	141.0	4377			149.65	−25.0	1.6	−3.94	1.27		
	148.7	4446			156.45	−33.6	0.3	−5.59	2.64		
	156.4	4445			159.85	−30.0	3.8	−5.13	0.26		
Aquitard Core	160.0	4806			165.25	−29.1	0.8	−6.26	1.19		
	165.4	4311			173.50	−29.2	1.7	−3.57	1.43		
	173.5	3598			179.35	−29.0	3.7	−3.20	0.93		
	179.2	3656	3.5	2340	184.90	−34.6	0.9	−5.90	2.28		
	185.0	3536			190.40	−30.2	2.5	−3.44	2.13		
	190.3	3627			195.10	−15.4	4.5	−0.13	2.94		
	194.9	2092			204.30	−23.6	0.3	−5.50	1.17		
	204.2	3269			208.40	−30.6	6.3	−6.37	2.89		
	208.3	3228	4.8	1525	214.50	−33.9	1.7	−3.98	0.77		
	214.3	3447	4.1	1890	219.70	−30.0	3.3	−3.37	1.76		
	214.8	3224			227.20	−31.8	1.9	−4.39	1.40		
	227.3	3113	3.9	1817	233.85	−32.5	1.1	−4.25	1.44		
	234.0	3357	3.7	2021	241.60	−31.2	1.9	−5.90	0.77		
	241.4	2643			248.75	−34.5	3.7	−3.80	1.23		
	248.6	2424	4.4	1243	251.80	−35.9	1.0	−3.57	1.15		
	252.5	2384	4.8	1127	257.90	−34.5	1.3	−3.82	1.53		
	258.1	2305	5.2	1008	260.30	−28.0	1.3	−1.82	3.75		
	260.4	2122			263.70	−37.5	3.2	−4.59	0.88		
	264.1	2217			268.40	−28.2	3.3	−4.13	1.12		
	268.3	2149	5.1	949	273.10	−31.7	4.0	−4.62	1.33		
	272.9	1911	4.8	901	279.00	−30.7	2.9	−6.31	1.61		
	279.2	1595	4.1	872	281.25	−32.0	1.9	−3.83	2.14		
	282.5	1517	3.5	966	285.60	−30.9	2.7	−5.81	0.87		
	285.8	1449	3.6	901	289.80	−33.8	5.0	−4.34	3.20		
	289.6	1623	4.5	814							
Nancy's Bore (confined)	324—344	2400	2.9	1865	324—344	−48.4		−6.64		2.6	0.1
BB2 piezometer (phreatic)	3.5—6.5	34000	17.0	4508	3.5—6.5	+0.5		+4.42		4	0.1
	22.1	20583	10.5	4397	22	−9.8	3.7	+3.89	1.91		
	27.2	20054	11.2	4033	27	−16.6	4.9	+2.88	1.61		
	32.4	17898			32	−14.9	5.1	+2.57	2.80		
	38.4	15607	10.4	3381	39	−17.6	3.1	+1.16	2.06		
	44.1	14283			44	−23.8	4.9	+1.55	3.09		
	48.7	11330	6.3	4047	48	−23.7	3.9	+1.36	3.35		
	54.1	9803	6.1	3633	54	−26.4	4.7	+0.10	1.09		
Aquitard Core	59.8	8547	4.9	3914	60	−28.4	5.3	−0.65	2.27		
	65.5	7501			66	−32.0	5.8	−1.77	1.43		
	71.5	5611	4.8	2612	71	−29.5	3.5	−2.41	1.09		
	75.2	4993			75	−30.4	3.5	−0.83	2.91		
	86.4	2911	3.9	1674	81	−35.0	3.2	−2.57	1.91		
	93.3	2322			86	−34.4	6.2	−2.48	2.64		
	97.2	1507	3.2	1078	93	−40.2	5.6	−3.87	1.59		
	102.1	1892			97	−37.8	3.8	−3.51	1.21		
					102	−39.8	7.5	−3.21	1.10		
Birthday Bore (confined)	131–148	2200	2.9	1709	131–148	−48.7		−6.51		2.9	0.1

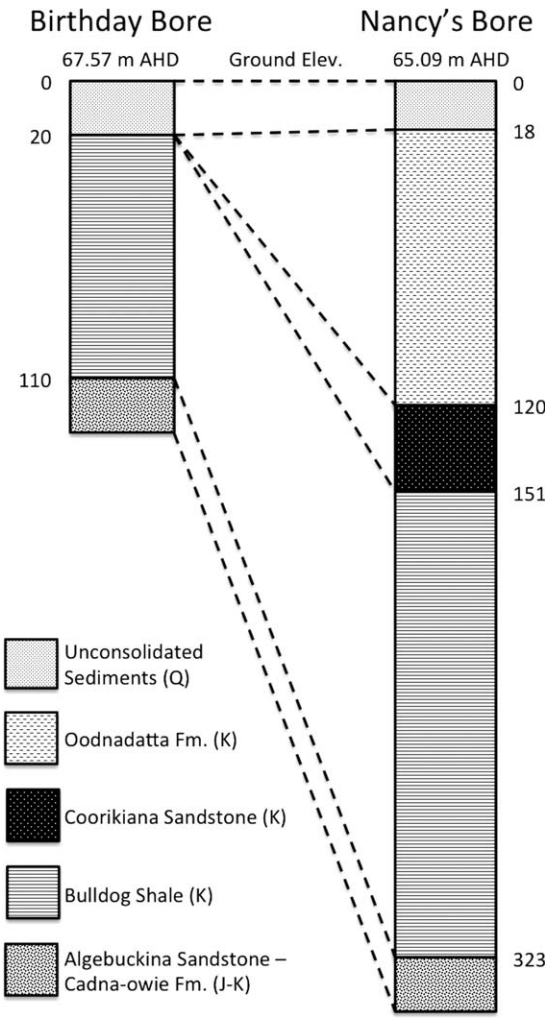

Figure 2. Schematic hydrostratigraphic cross-section between Birthday Bore and Nancy's Bore (locations shown in Figure 1). AHD is Australian Height Datum and is approximately equal to mean sea level. Depths on sides are in metres below ground level.

piezometers at NB2 due to excessive contamination from drilling mud. Samples for carbon-14 analysis were collected in 1.25 L PET bottles and transferred to the Isotope Analytical Service at CSIRO Land and Water (Adelaide, Australia) for conversion of dissolved inorganic carbon to carbon dioxide gas, and subsequent measurement by Accelerator Mass Spectrometry at the Australian National University, Canberra. Groundwater samples were analyzed for major ion concentrations (including Cl^- and Br^-) by inductively coupled plasma-optical emission spectroscopy and liquid ion chromatography, and for δ^2H and $\delta^{18}O$ by Isotope Ratio Mass Spectrometry on a Europa® Geo 20-20 stable isotope mass spectrometer; both analyses were also undertaken at CSIRO Land and Water, Adelaide.

3.4. Modeling Approach and Input Parameters

[25] Equation (1) was solved numerically using MT3DMS [*Zheng and Wang*, 1999]. The finite difference groundwater flow model MODFLOW-96 [*MacDonald and Harbaugh*, 1996] was used to produce a steady-state flow field at each site by assigning specified head boundary conditions at the top (phreatic aquifer) and bottom (J-K aquifer) of the model domains, with constant values corresponding to measured water levels and artesian heads in April 2011 (Table 2). The assumption of steady state flow conditions is based on two lines of evidence. First, long-term denudation rates for the western Lake Eyre Basin and surrounds are understood to be in the range of 0–2 m/Ma over the Cenozoic [*Gale*, 1992]. Therefore, erosional unloading and any associated reduction of hydraulic head in the middle of the aquitard sequence—as observed in other Cretaceous aquitards (e.g., *Neuzil* [1993])—can be considered negligible. This is supported by porewater pressure data obtained from vibrating wire piezometers grouted in the aquitard, which show no evidence of anomalous pressures [*Smerdon et al*., 2012]. Second, it is likely the upward hydraulic gradient that exists between the shallow, phreatic aquifer and the J-K aquifer in this part of the GAB has remained relatively constant over time. Both core sites are located less than 100 km from the main discharge area for the entire GAB flow system, a series of playa lakes and mound springs near the southwest margin of the basin. This discharge area can be considered a hinge point about which the long, flat, horizontal hydraulic gradient for the J-K aquifer pivots. Therefore, any changes to the up-gradient recharge or flow characteristics of this system will produce a delayed and very subdued effect on the absolute hydraulic head at the two core sites. Furthermore, it is likely the shallow phreatic aquifer has persisted over at least the last 150 ka, albeit the water table depth would have varied slightly in response to different pluvial conditions.

[26] The entire aquitard sequence at each site was represented in the MODFLOW-MT3DMS models as a single row and single column of cells, with multiple layers having a uniform thickness of one metre (i.e., 306 layers for NB2 and 90 layers for BB2). All aquitard cells were assigned constant hydraulic parameters, including hydraulic conductivity (K) and total porosity, with the latter based on measured data ($\mu = 0.40,\ \sigma = 0.06,\ n = 62$). One-dimensional (vertical) flow and transport was considered appropriate for these simulations because the vertical hydraulic gradient through the aquitard (0.11–0.15) is more than three orders of magnitude greater than the horizontal hydraulic gradient in the aquifers (<0.0005; *Habermehl and Lau*, 1997). Additionally, lateral diffusion would only be important if a horizontal concentration gradient were in existence, which is highly unlikely given the near-horizontal stratigraphy and extensive distances to recharge or discharge boundaries. Because only vertical flow and transport was simulated in the models, the steady-state flow across individual aquitard layers is constant and controlled by the lowest K layers of the entire sequence, regardless of the changes in stratigraphy. Hence, only a single value of K_v was applied to represent the combined aquitard sequence for each core.

[27] Based on previous estimates of K, and thus fluid velocity (v_z), obtained using both noble gases [*Gardner et al*., 2012] and hydraulic methods [*Smerdon et al*., 2012] it was anticipated that transport of Cl^- and δ^2H would be dominated by diffusion rather than advection (i.e., Peclet numbers less than one) and that mechanical dispersion would be negligible compared to diffusion (i.e., $D_p >> \alpha_z v_z$ in equation (2)). Hence dispersivity was set at zero for these

Table 2. Initial Concentrations and Boundary Conditions (BC) Adopted for Chloride and Deuterium Simulations at Nancy's Bore and Birthday Bore

		Upper BC (Phreatic)		Lower BC (Confined)	
Site/Tracer/Time BP	Initial Conc.	Flow	Transport	Flow	Transport
Nancy's Bore					
Chloride	500 mg L^{-1}	Fixed Head	Fixed Conc.	Fixed Head	Fixed Conc.
3.12–0.12 Ma		−12.0 m	9000 mg L^{-1}	+25.23 m	500 mg L^{-1}
120–20 ka			500 mg L^{-1}		500 mg L^{-1}
20–10 ka			6000 mg L^{-1}		500 mg L^{-1}
10–0 ka			6000 mg L^{-1}		2400 mg L^{-1}
Deuterium	−40‰		Fixed Conc.		Fixed Conc.
4.12–0.12 Ma			−8‰		−40‰
120–20 ka			−40‰		−40‰
20–10 ka			−15‰		−40‰
10–0 ka			−15‰		−48.4‰
Birthday Bore					
Chloride	500 mg L^{-1}	Fixed Head	Const. flux	Fixed Head	Fixed Conc.
70–20 ka		−3.5 m	58 kg ha^{-1} a^{-1}	+16.13 m	500 mg L^{-1}
20–0 ka			58 kg ha^{-1} a^{-1}		2200 mg L^{-1}
Deuterium	−40‰		Fixed Conc.		Fixed Conc.
70–20 ka			+0.7‰		−40‰
20–0 ka			+0.7‰		−48.5‰

models. An Upstream Finite Difference (UFD) scheme was used in MT3DMS rather than any of the more conventional Method of Characteristics schemes commonly used for advection-dominated systems. UFD only leads to numerical dispersion in advection dominated problems [*Zheng and Wang*, 1999], and others have shown that standard finite difference schemes, with either upstream or central weighting schemes, are appropriate provided the grid Peclet number is less than four [*Zheng and Bennett*, 1995], a criterion easily met for this study.

[28] MT3DMS requires the input of an "effective diffusion coefficient" however close inspection of the mathematics in the user's manual [*Zheng and Wang*, 1999] reveals that this parameter is actually equivalent to D_p (i.e., D_e/η_e). We assumed that for HDO the effective porosity was equal to the average value of total porosity from both cores (i.e., $\eta_e=\eta=0.40$), and due to the high ionic strength of the aquitard pore waters (0.1–0.3 M; data not presented) the same approach was adopted for simulating Cl^- transport. Adopting free water diffusion coefficients (D_0) of 1.71×10^{-9} m^2s^{-1} for Cl^- at 18 °C [*Li and Gregory*, 1974] and 2.27×10^{-9} m^2s^{-1} for HDO at 25 °C [*Mills*, 1973], and a value of $m = 2.3$ enabled the estimation of D_e values using equation (7). Then using equation (9) and the average measured in-situ temperature of both cores (30.6 °C, *Smerdon et al*., 2012] we obtained average temperature-corrected D_e values of 2.9×10^{-10} m^2s^{-1} and 3.8×10^{-10} m^2s^{-1} for Cl^- and HDO (respectively), which were subsequently converted to D_p for input to MT3DMS. A discussion on the potential errors associated with this approach for estimating D_e, and implications for solute transport modeling, is presented later. Details of the concentration boundary conditions used for each tracer and site are provided in the following section.

[29] The general modeling approach for each site was to first run series of steady-state flow simulations with the head boundary conditions described above and a range of possible values for vertical hydraulic conductivity (K_v), based on previous estimates obtained using terrigenic helium-4 profiles [*Gardner et al*., 2012] and pore pressure recovery data [*Smerdon et al*., 2012]. The velocity vectors from these flow simulations were then fed into the transport simulations, with various concentration boundary conditions, to determine the most appropriate value of K_v (and thus fluid flux) and timescales for evolution of the profiles. Given the uncertainties in transport properties η_e and D_e described above, these parameters were not altered during the tracer simulations.

4. Results and Discussion

4.1. Evidence of Uncontaminated Core

[30] Pore water δ^2H and $\delta^{18}O$ compositions in the BB2 core range from −40.2 to −9.8‰ Vienna SMOW (VSMOW) and −3.9 to +3.9‰ VSMOW, respectively (Table 1). Similarly, pore water compositions in the NB2 core range from −37.5 to −15.4‰ VSMOW and −6.4 to −0.1‰ VSMOW, respectively. The samples from BB2 display a linear trend on a conventional δ^2H-$\delta^{18}O$ plot that is characteristic of evaporative enrichment, whereas the samples from NB2 seem to cluster with no apparent trend (Figure 3). While highly variable, the δ^2H composition of spiked drilling mud (+24.3 to +65.2‰ VSMOW, Figure 3) was always significantly more enriched than the measured pore water compositions, providing confidence that the core was not contaminated during drilling.

4.2. Birthday Bore—Chloride

[31] Pore water Cl^- data from the BB2 core ranges from 1507 to 34000 mg L^{-1} (Table 1) and exhibits a classical curve-shaped advection-diffusion profile, generally plotting between measured groundwater Cl^- concentrations in the phreatic and J-K aquifers (Figure 4). The only apparent anomaly in this profile is the deepest pore water samples (>80 m) have lower Cl^- concentrations than the measured groundwater value for the underlying confined aquifer,

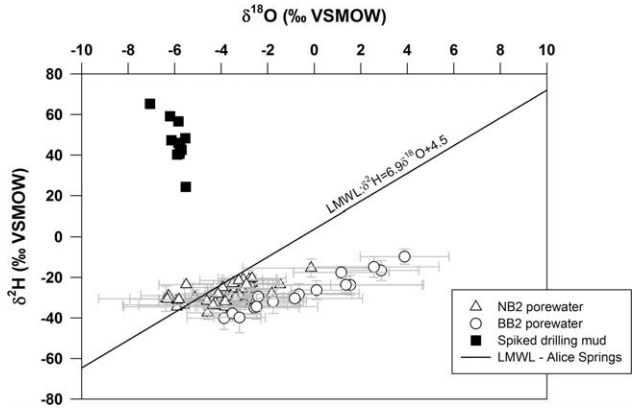

Figure 3. Stable H/O isotope composition of aquitard pore water and drilling mud.

suggesting this boundary condition has changed recently. The measured carbon-14 activity for Birthday Bore (2.9 pmC; Table 1) corresponds to an apparent, uncorrected groundwater age of about 28 ka; a result that was not expected for groundwater at the discharge end of the massive GAB. We therefore propose that recharge to the J-K aquifer on the southwest margin of the GAB occurred locally during the late Pleistocene—perhaps at narrow outcrop areas to the west—rather than by lateral inflow from the northeast.

[32] Three different conceptual models for the Cl^- profile at BB2 core were evaluated through numerical simulation. Comparison of different simulation results with measured data was largely qualitative; however, the ultimate selection of the most appropriate conceptual model was based on (a) the general shape of the simulated profile, and (b) whether it was justifiable from a hydrogeological perspective. The first model assumed constant concentration boundary conditions for both the phreatic and J-K aquifers, with applied values of 34 000 mg L^{-1} and 1 500 mg L^{-1}, respectively. By applying a constant, low initial Cl^- concentration throughout the aquitard of 1500 mg L^{-1}, the measured BB2 pore water Cl^- profile could be adequately simulated with this model (Figure 4a) providing $K_v < 8.5 \times 10^{-12}$ m s^{-1}. The problem with this model, however, is the choice of boundary conditions. While constant concentration is probably justifiable for the J-K aquifer, due to long groundwater flow paths and thus long-term stability in water quality, there is no reasonable justification for fixing the concentration of the phreatic aquifer for several hundred thousand years.

[33] The second model investigated whether progressive evaporation from the phreatic aquifer, and concomitant increase in Cl^- concentration, could explain the measured BB2 Cl^- profile. This was achieved by assigning a constant concentration boundary condition for the J-K aquifer (as per the first model) and no solute transport boundary condition for the phreatic aquifer (i.e., effectively zero solute flux). Adopting a low initial Cl^- concentration of 1500 mg L^{-1} for the entire aquitard, this model failed to reproduce the shape of the measured data regardless of the K_v value and despite a long model simulation time of 1 Ma (Figure 4b). For low values of $K_v < 1 \times 10^{-11}$ m s^{-1}, the simulated Cl^- profile was essentially unchanged from the initial condition, as any build-up of concentration in the phreatic aquifer was outpaced by downward diffusive loss. The only way to build Cl^- concentration at the top of the profile to anything like measured values was to implement a high $K_v > 1 \times 10^{-10}$ m s^{-1}; however, this still resulted in significant under-prediction of Cl^- concentration for the middle two-thirds of the profile.

[34] Therefore, a third model was conceptualized in which an external source of Cl^- was invoked and applied as the upper boundary condition of the model. The remainder of this section evaluates the possible source of this salt and the flux required to evolve the BB2 profile to its current state.

[35] Computing Cl^-/Br^- ratios of water samples is a technique often used to determine the sources of salts

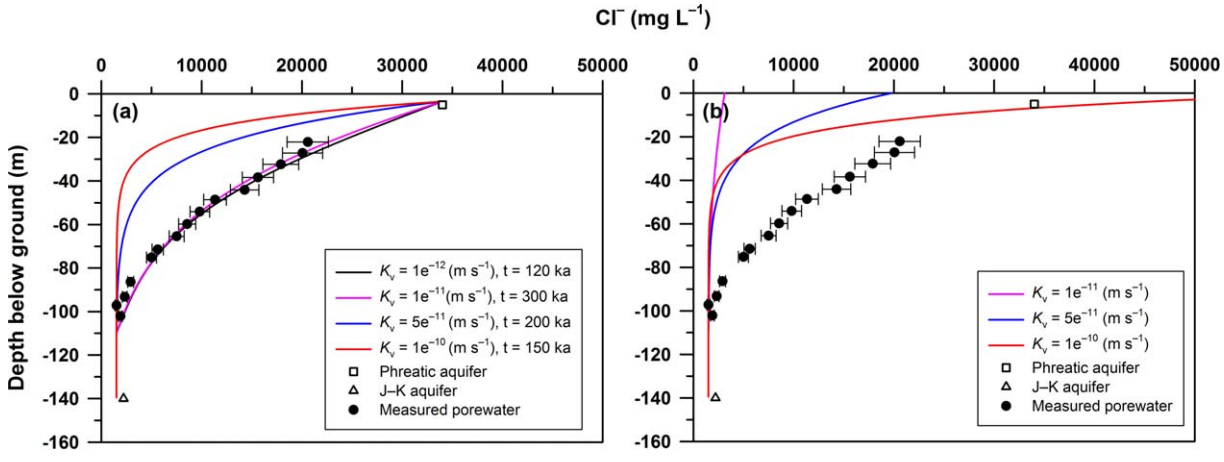

Figure 4. Measured and modeled (preliminary) chloride concentration in aquitard pore water, phreatic and confined aquifers at Birthday Bore. Analytical errors for aquifer samples are within the size of the symbols. (a) Simulated steady-state profile using fixed concentration for both upper and lower boundary conditions. (b) Simulated profile after 1 Ma using a fixed concentration for the lower boundary condition and a zero solute flux for the upper boundary condition, allowing Cl^- to accumulate near the top of the aquitard due to upward groundwater flow.

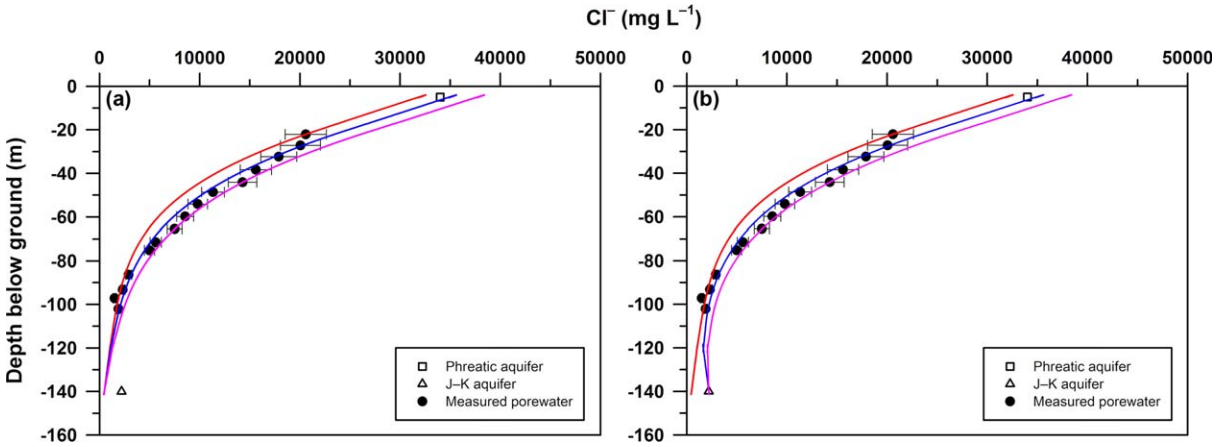

Figure 5. Measured and modeled (final) chloride concentration in aquitard pore water, phreatic and confined aquifers at Birthday Bore. Analytical errors for aquifer samples are within the size of the symbols. (a) Measured data and simulated profile after 50 ka (red line), 60 ka (blue line), and 70 ka (pink line) using a fixed concentration in the J-K aquifer and a constant salt flux to the phreatic aquifer. (b) Same simulation (red line 50 ka) but applying a higher Cl^- concentration (as measured) in the J-K aquifer after 50 ka (blue line 60 ka; pink line 70 ka).

containing these elements, because atom ratios greater than that of seawater (typically ~660; *Davis et al*., 1998) are indicative of halite dissolution. Despite Br^- having long been regarded as a conservative anion, several recent studies in arid environments—including one from the Lake Eyre Basin [*Tweed et al*., 2011] and one from Abu Dhabi [*Wood and Sanford*, 2007]—have speculated that Br^- may not behave conservatively in these environments. Processes such as adsorption onto iron and manganese oxides, uptake during plant transpiration and halite precipitation, and degassing to the troposphere are now recognized constraints for using Br^- in hydrological applications [*Tweed et al*., 2011].

[36] While the above processes may limit the use of Br^- as a quantitative geochemical tracer in arid settings, the Cl^-/Br^- atom ratio is still likely to be a useful indicator of whether halite dissolution is responsible for the high Cl^- concentrations observed in the phreatic aquifer and aquitard pore water at BB2. The ratios listed in Table 1 reveal a range from 1078 to 4397 for the pore water samples, which are significantly higher than the seawater value of ~660, suggesting halite is a likely source of Cl^- for the BB2 site.

[37] The only current source of estimates for the Cl^- flux to the land surface in this location is the Geoscience Australia website (http://mapconnect.ga.gov.au/MapConnectIn/Groundwater/), which yields a mean value of 2.09 kg ha^{-1} a^{-1} (range, 1.38–7.64 kg ha^{-1} a^{-1}). An alternative approach for estimating the Cl^- flux required to build the measured profile at BB2 is to use Fick's first law to estimate the Cl^- flux (J) to the water table:

$$J = -D\frac{\partial c}{\partial z}. \tag{10}$$

[38] Using the adopted value of $D_e = 2.9 \times 10^{-10}$ $m^2 s^{-1}$ and a vertical concentration gradient of 400 mg L^{-1} m^{-1} for the upper part of the profile, the Cl^- flux is estimated to be 37 kg ha^{-1} a^{-1}, which is significantly higher than the theoretical estimates above.

[39] Numerous MODFLOW-MT3DMS simulations were performed using a range of values for K_v (1×10^{-13} to 1×10^{-11} m s^{-1}) and applying a salt flux to the upper boundary (2, 37, 50, 58, and 66 kg ha^{-1} a^{-1}). In order to implement a constant salt flux at the upper boundary, which is also a constant head boundary, the model mesh was refined into three columns. This enabled constant heads to be assigned to the outer two cells and constant recharge with specified concentrations assigned to the central cell. An optimal fit between simulated and measured Cl^- data was achieved with a K_v of $\sim 1 \times 10^{-13}$ m s^{-1} and a salt flux of 58 kg ha^{-1} a^{-1} (Figure 5a). Refer to Table 2 and Figure 6 for a summary of boundary conditions. The adopted value of K_v falls between two independent estimates provided by *Smerdon et al*. [2012] (i.e., $K_v = 0.4 \times 10^{-13}$ m s^{-1}) and *Gardner et al*. [2012] (i.e., $K_v = 5 \times 10^{-11}$ m s^{-1}). Subsequent sensitivity analysis of the simulated Cl^- profile—achieved by holding the salt flux constant and varying K_v—revealed that the model cannot reliably resolve K_v below $\sim 1 \times 10^{-12}$ m s^{-1} (Figure 7). This is because the downward solute flux by diffusion starts to outpace the upward solute flux by advection when $K_v < 1 \times 10^{-12}$ m s^{-1}.

[40] The high adopted salt flux suggests there is a substantial import of salt to the area, most likely due to windblown dust from nearby playa lakes, as observed in a similar study of a saline lake basin in southern Texas, USA [*Wood and Sanford*, 1995]. This external source of salt is flushed into the water table following episodic rain events. The simulated timeframe required to develop the measured Cl^- profile is somewhere in the range of 60–70 ka, with the best fit arguably toward the lower end of this range (Figure 5a). *Magee et al*. [2004] suggest that major deflation of Lake Eyre between 60 and 40 ka before present (BP) resulted in the excavation of the modern playa and a major

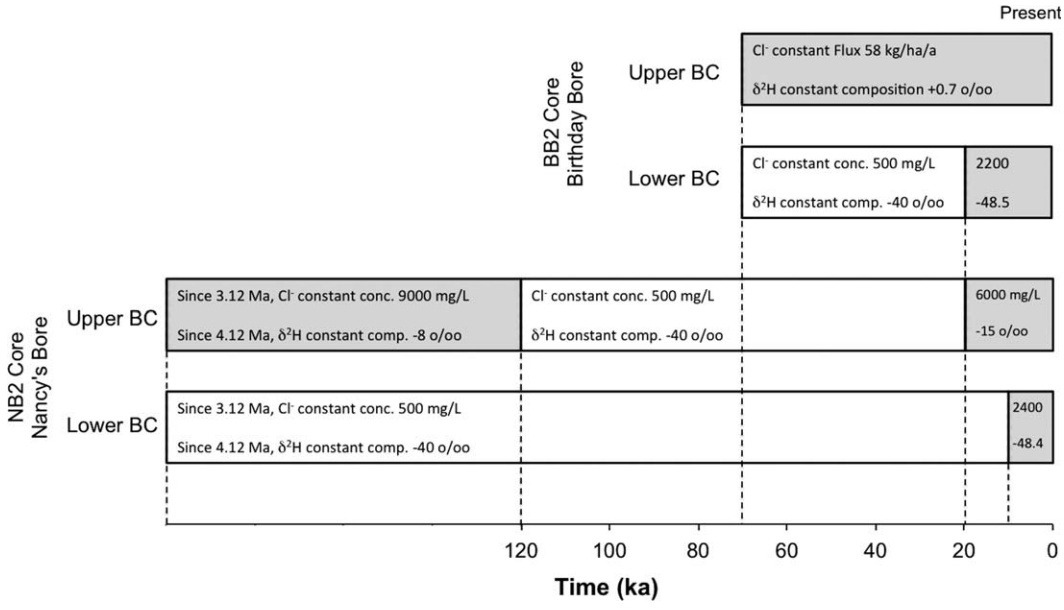

Figure 6. Graphical representation of upper and lower concentration boundary conditions adopted for Birthday Bore and Nancy's Bore simulations.

change in local hydrological conditions, including the lowering of water tables. Therefore, the simulation timeframe of ~60 ka for development of the Cl^- profile is consistent with the onset of significant salt remobilization in the region.

[41] The initial simulations of Cl^- at BB2 were rerun for 70 ka but with a higher Cl^- concentration, equivalent to the measured value, in the J-K aquifer for the last 20 ka. These simulations suggest it is unlikely the current Cl^- concentration in the J-K aquifer has existed for much more than the last ~10 ka (Figure 5b).

4.3. Birthday Bore—Deuterium

[42] The δ^2H profile at BB2 (Figure 8) exhibits the same shape as the Cl^- profile, but with greater measurement uncertainty for individual samples. The δ^2H values for the lower part of the aquitard are significantly more enriched than groundwater in the J-K aquifer, suggesting the groundwater in this aquifer had more enriched δ^2H composition in the recent past.

[43] The modeling approach for the δ^2H profile was to apply constant δ^2H composition boundary conditions for both the phreatic and J-K aquifers (Table 2). While this type of boundary condition was considered to be less than ideal for the phreatic aquifer when modeling the Cl^- profile, a conceptual model of the site being a local groundwater discharge zone (discussed later) means that δ^2H composition could be more constant over time than Cl^-.

[44] Using the adopted K_v value and simulation times derived from the Cl^- model, the simulated δ^2H profile provides a good match with the (noisy) measured data (Figure 8a). One could argue that the 50 ka profile provides a better match than the 70 ka profile; however, these simulations are very sensitive to the choice of the lower boundary condition, and thus the timeframes for development of the δ^2H profile cannot be resolved from the model. Likewise, changing the lower boundary condition to the more depleted (measured) δ^2H value for the last 20 ka provided inconclusive evidence for the timescale over which this condition has existed, although it could be significantly greater than 10 ka (Figure 8b).

4.4. Nancy's Bore—Chloride

[45] Pore water Cl^- data from the NB2 core ranges from 1517 to 5355 mgL^{-1} (Table 1) and exhibits a nonlinear trend with a freshening shift in the upper part of the profile (Figure 9a). Deviation of the profile away from a linear trend is roughly coincident with the Coorikiana Sandstone, suggesting this formation may have some control on solute transport through the aquitard (discussed further below).

[46] The Cl^- concentration in the upper, phreatic aquifer was not measured due to failure of the piezometer at the site; hence, an assumed value of 6000 mg/L was adopted based on the trend in Cl^- concentration in the uppermost

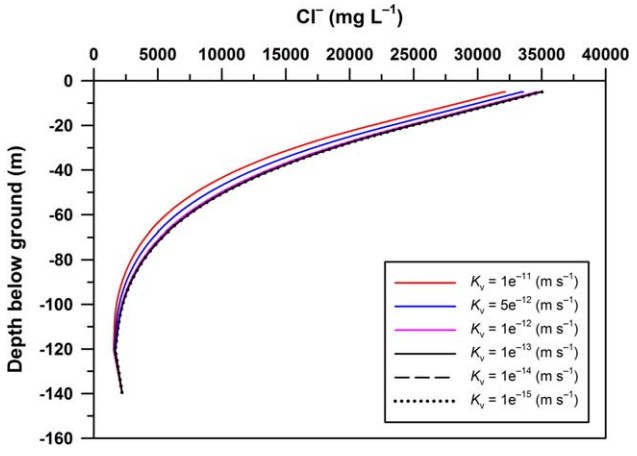

Figure 7. Sensitivity of simulated Cl^- profile at Birthday Bore to K_v (Cl^- flux at surface held constant). Profiles are indistinguishable for $K_v < 1 \times 10^{-12}$ m s^{-1}.

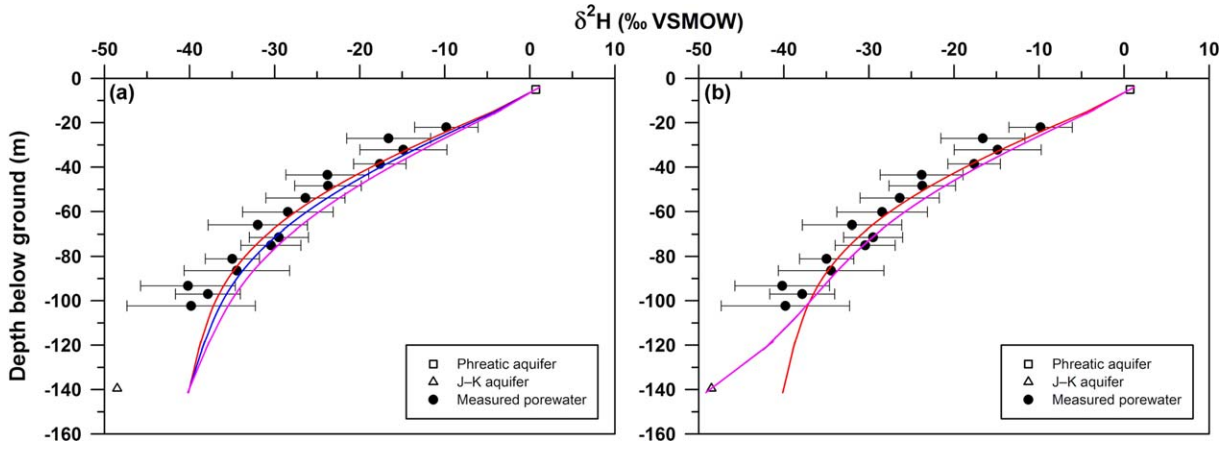

Figure 8. Measured and modeled δ^2H composition of aquitard pore water, phreatic and confined aquifers at Birthday Bore. Analytical errors for aquifer samples are within the size of the symbols. (a) Measured data and simulated profile after 50 ka (red line), 60 ka (blue line), and 70 ka (pink line) using a fixed concentration for both the phreatic and J-K aquifer. (b) Same simulation (red line 50 ka) but applying a more depleted δ^2H value (as measured) in the J-K aquifer after 50 ka (pink line 70 ka).

section of the aquitard (Table 2, and hollow square in Figure 9a). Measured Cl^- concentration in the J-K aquifer (2400 mg/L) is much higher than that of pore water in the lower part of the aquitard. This is consistent with the observation at BB2, providing further evidence that the J-K aquifer was fresher in the past.

[47] The lower half of the Cl^- profile has an approximately linear trend, suggesting a long-term (perhaps steady-state) diffusion profile. The upper half of the profile could be interpreted in several different ways. One possible explanation is that a peak in Cl^- concentration occurs within the Coorikiana Sandstone as a result of lateral groundwater inflow with relatively high Cl^-, and this Cl^- is diffusing upwards and downwards away from the peak into zones of lower Cl^- concentration introduced during past conditions.

[48] Previous research in a thick, regional aquitard system has shown how thin, sand-filled layers or conduits may be responsible for propagating chloride "halos" laterally through an aquitard [*Harrington et al*., 2007]. In order for this process to be detected as a single peak in 1-D porewater profiles down-gradient of a source, the amount of solute mass and rate of lateral advective transport must be sufficiently large to outpace diffusive loss of solute into the adjacent aquitard(s).

[49] *Moore and Pitt* [1985] describe the Coorikiana Formation as a predominantly calcareous, clayey, very fine to fine-grained sandstone and sandy siltstone with minor siltstone interbeds. This description is consistent with observations of the core at the time of drilling and down-hole geophysical logging [*Smerdon et al*., 2012], which revealed approximately 1.5 m of medium-grained sandstone that could be considered an aquifer.

[50] When these permeability characteristics are coupled with the very flat hydraulic gradients observed throughout the region (typically <0.0004) and a distance of almost 10 km to the nearest outcrop of the Coorikiana Sandstone, it seems unlikely this mechanism could be responsible for the observed Cl^- profile at NB2.

[51] An alternative hypothesis is that the upper half of the profile has been affected by alternating fresh and saline phases in the shallow phreatic aquifer.

[52] The large ephemeral playa Lake Eyre, situated only ~40 km east of NB2, has been the subject of intense sediment chronology and palaeohydrology research over the last three decades. *Bowler* [1978; cited in *Kotwicki*, 1986] suggested that Lake Dieri (ancestral Greater Lake Eyre) underwent a constant phase of filling between ~45 ka and ~25 ka. Subsequently, *Magee et al*. [1995] determined a detailed chronology of Quaternary lake hydrology and stratigraphy using a range of sediment dating techniques, including thermoluminescence, uranium/thorium disequilibrium, amino acid racemization (AAR), and carbon-14. They identified the wettest phase in the last 130 ka was during the last interglacial between 130 and 90 ka BP, at which time the lake was up to 25 m deep. *DeVogel et al*. [2004] have since calculated that during this highstand phase Lake Eyre covered nearly 35,000 km^2, more than three times the area of the current playa. *Magee et al*. [1995] also identified a lacustral phase between 90 and 70 ka BP, followed by a period of playa deflation (60–50 ka BP), another lacustral phase (50–25 ka BP), and playa deflation (25–10 ka BP). During the Holocene, a shallow lacustrine phase occurred from about 10–4 ka BP before there was a shift to the ephemeral playa phase observed today (i.e., 3–0 ka BP).

[53] *Magee and Miller* [1998] reported AAR and AMS carbon-14 analyses of mollusc shell and bird eggshell, revealing that Lake Eyre was at least as dry as it is today between 35 and 10 ka BP. More recently, *Magee et al*. [2004] constructed a 150 ka chronology for the lake, confirming the following phases, which are summarized in Figure 10: greatest aridity (150–130 ka BP), deepest perennial lake (130–110 ka BP), brief drying, refilling (100–75 ka BP), drying and deflation (75–70 ka BP), lacustrine conditions (65–60 ka BP), drying and significant deflation (60–40 ka BP), minor low-level perennial lake (~40 ka BP), drying and minor deflation (35–12 ka BP), low-level perennial lake (12–4 ka BP), modern ephemerally flooded playa (4–0 ka BP).

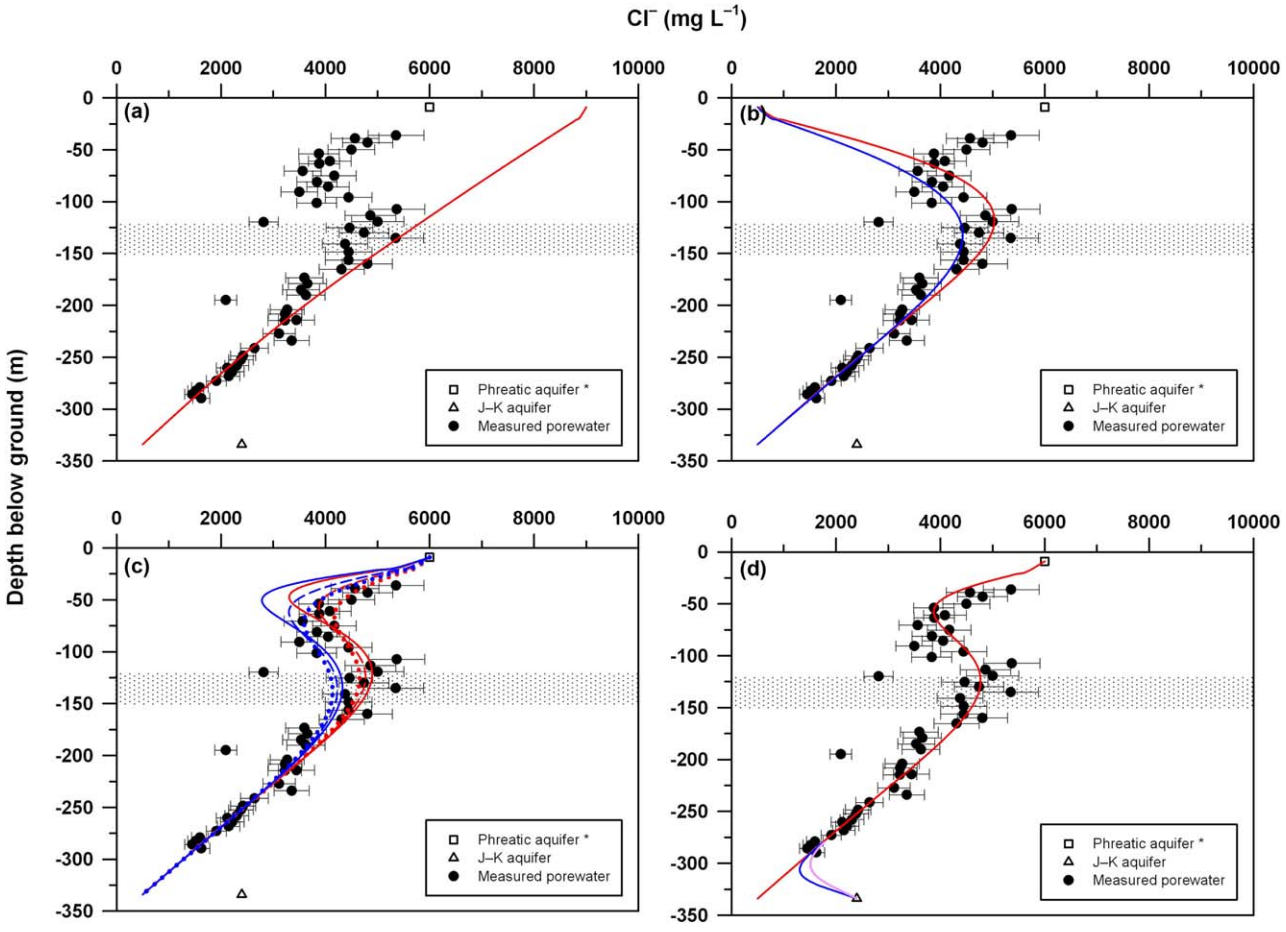

Figure 9. Measured and modeled chloride concentration in aquitard pore water and confined aquifer at Nancy's Bore. Analytical error for aquifer sample is within the size of the symbol. Concentration of phreatic aquifer is estimated, as indicated by the asterisk. Shaded zone corresponds to the location of the Coorikiana Sandstone formation. (a) Measured data and initial steady state (>3 Ma) simulation. (b) Simulated profiles after 100 ka (red line) and 150 ka (blue line) with a fresher upper boundary condition. (c) Simulated profiles after a further 10 ka (solid line), 20 ka (dashed line), and 30 ka (dotted line) with a more saline upper boundary condition. (d) Same simulation (red line 120 ka) but applying a higher Cl^- concentration (as measured) in the J-K aquifer after 110 ka (blue line 115 ka; pink line 120 ka).

[54] Similar research has been undertaken in playa Lake Frome, situated 350 km further southeast from Lake Eyre, focusing on the palaeohydrology toward the end of the Pleistocene and during the Holocene. Using late Quaternary pollen records, *Singh* [1981] identified three wetter periods between 9.5 and 8 ka BP, 7 and 4.2 ka BP, and 2.2 and 0 ka BP. *Ullman and McLeod* [1986] then investigated Na^+ concentrations in stratigraphically preserved gypsum and found evidence for three other distinct periods of lake filling: ~17 ka BP, between 15 and 13.5 ka BP, and between 13 and 11 ka BP.

[55] To determine whether palaeohydrological changes in the phreatic aquifer could explain the measured Cl^- profile at NB2, we investigated the effects of transient solute transport boundary conditions on the modeling results. The approach was to start with a steady-state model of Cl^- distribution to represent (at least) the lower half of the profile. Constant head and constant concentration upper and lower boundary conditions were assumed (Table 2) and an

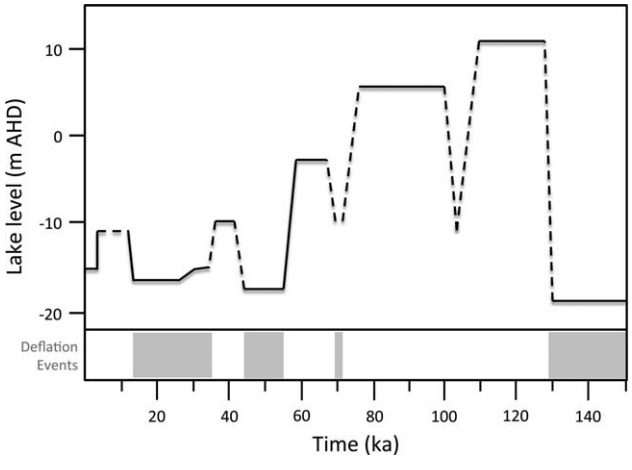

Figure 10. Palaeohydrology of Lake Eyre, reproduced from *Magee et al*. [2004]. (AHD is Australian Height Datum and is approximately equal to mean sea level.)

optimal K_v was determined by trialing values derived from helium-4 profiles [*Gardner et al*., 2012] and aquitard hydraulic responses [*Smerdon et al*., 2012].

[56] Using the steady-state model results as a new initial condition, a series of simulations were performed, first by implementing a freshening phase (i.e., lower Cl^-) in the phreatic aquifer, then a more saline phase (i.e., higher Cl^-) in the phreatic aquifer (Figure 6). The decision to apply only one freshening phase and one salinization phase, rather than multiple phases consistent with palaeohydrology records from Lake Eyre, reflected the fact that multiple events could not be deciphered from the pore water Cl^- data. Finally, a more saline lower boundary condition was applied toward the end of these simulations to understand the likely timescale over which conditions have changed in the J-K aquifer.

[57] An optimal value for vertical hydraulic conductivity (K_v) of 1×10^{-13} m s^{-1} was determined through trial and error, which is the same value as determined for the BB2 core and compares well with estimates reported by both *Smerdon et al*. [2012] ($K_v = 1.2 \times 10^{-13}$ m s^{-1}) and *Gardner et al*. [2012] ($K_v < 1 \times 10^{-12}$ m s^{-1}). Applying any higher value of K_v produced poor matches in terms of the shape of measured Cl^- profile, regardless of the simulation time. Furthermore, there was no justification for changing K_v with depth through the aquitard sequence. Using a K_v of 1×10^{-13} m s^{-1}, the lower part of the Cl^- profile takes >3 Ma to evolve from a constant initial condition (Figure 9a).

[58] Following an instantaneous change to fresher conditions in the phreatic aquifer, the Cl^- profile between about 70 m and 170 m takes in the range of 100–150 ka to develop (Figure 9b), coincident with the transition from middle to late Pleistocene (~120 ka BP) and the onset of the wettest phase (~130 ka BP, *Magee et al*. [2004]; see Figure 10).

[59] Using both the 100 ka and 150 ka simulations as new initial conditions and applying a subsequent more saline boundary condition in the phreatic aquifer suggested the shorter timescale (i.e., 100 ka) is probably more realistic, and that these conditions have persisted at least since the start of the Holocene, possibly for the last ~20 ka (Figure 9c). This timing is consistent with the extended period of dryness and deflation in Lake Eyre (35–12 ka BP, *Magee et al*. [2004]; see Figure 10).

[60] This simple model, utilizing one phase of phreatic aquifer freshening (~120 ka to ~20 ka BP) followed by one phase of phreatic aquifer salinization (~20 ka BP to present), provides a very good fit to the measured pore water Cl^- profile. While previous researchers have identified several alternating phases of wetting and drying throughout the late Quaternary, these individual phases cannot be resolved from the pore water profile, and thus were not modeled. However, the impact of multiple freshening and salinization phases within the last 120 ka would be a disturbance to the upper part of the pore water Cl^- profile, changing it from a smooth curve to something more noisy; this may explain the relatively large scatter in Cl^- concentration observed in the uppermost part of the aquitard.

[61] When simulating the evolution of the pore water Cl^- profile—including both the initial steady-state simulation and subsequent time-dependent boundary concentration simulations—it was necessary to specify a constant concentration in the J-K aquifer of 500 mg L^{-1}, which is significantly fresher than the value measured at Nancy's Bore (2400 mg L^{-1}). This suggests Cl^- concentration in the confined aquifer changed relatively recently compared to the timescale required for evolution of the profile. The carbon-14 activity of dissolved inorganic carbon in groundwater sampled from the same bore (2.6 pmC; Table 1) corresponds to an apparent, uncorrected groundwater age of about 29 ka, again supporting the hypothesis of local recharge to the J-K aquifer during the late Pleistocene.

[62] Several model scenarios were used to estimate the length of time over which the higher Cl^- concentration observed in the J-K aquifer may have existed. These scenarios involved rerunning the simulations used previously to represent salinization of the phreatic aquifer (Figure 9c), but with the lower boundary condition changed to 2400 mg L^{-1} for different lengths of time toward the end of the simulation. The results indicate that the higher Cl^- concentration in the J-K aquifer is unlikely to have existed for much more than ~10 ka because any longer timeframes would have caused the linear pore water Cl^- profile to start curving toward this concentration (Figure 9d).

4.5. Nancy's Bore—Deuterium

[63] The δ^2H profile at NB2 (Figure 11a) and accompanying $\delta^{18}O$ profile (not shown) exhibits far greater noise than the Cl^- profile, reflecting large uncertainties in the analytical procedure, and the relatively small range of δ^2H values (less than a factor of two) compared with Cl^- concentrations (almost a factor of four). The range in δ^2H values is also significantly narrower than most ranges observed in aquitard studies in North America (e.g., *Hendry et al*. [2011]) and Europe (e.g., *Mazurek et al*. [2011]).

[64] Nevertheless, the δ^2H profile exhibits similar trends to those observed in the Cl^- profile, including a possible shift to more depleted values in the Oodnadatta Formation. The only significant difference between the two profiles is that δ^2H values for the lower part of the aquitard are more enriched than groundwater in the J-K aquifer, whereas Cl^- concentrations in the aquitard are fresher than groundwater in the aquifer.

[65] Given the noisy nature of the observed pore water δ^2H profile, the modeling approach was to implement the same steady-state hydraulic conditions, and time-dependent boundary condition regime as used to model the Cl^- profile. Details of the prescribed boundary conditions are listed in Table 2 and summarized in Figure 6.

[66] The modeled δ^2H profiles do not match measurements as well as the modeled Cl^- profile. The initial steady-state simulation (Figure 11a) does capture the trend for most of the lower half of the profile, except for the deepest pore water samples. Subsequent simulations with varying upper boundary conditions (Figure 11b) seem to represent the upper half of the profile, although the analytical uncertainty in the pore water δ^2H measurements precludes this analysis from being meaningful.

[67] Measured δ^2H values from the deepest part of the aquitard (>260 m) are significantly enriched relative to both aquitard pore water immediately above this zone, and groundwater in the aquifer below. This suggests the groundwater δ^2H composition for the J-K aquifer may have

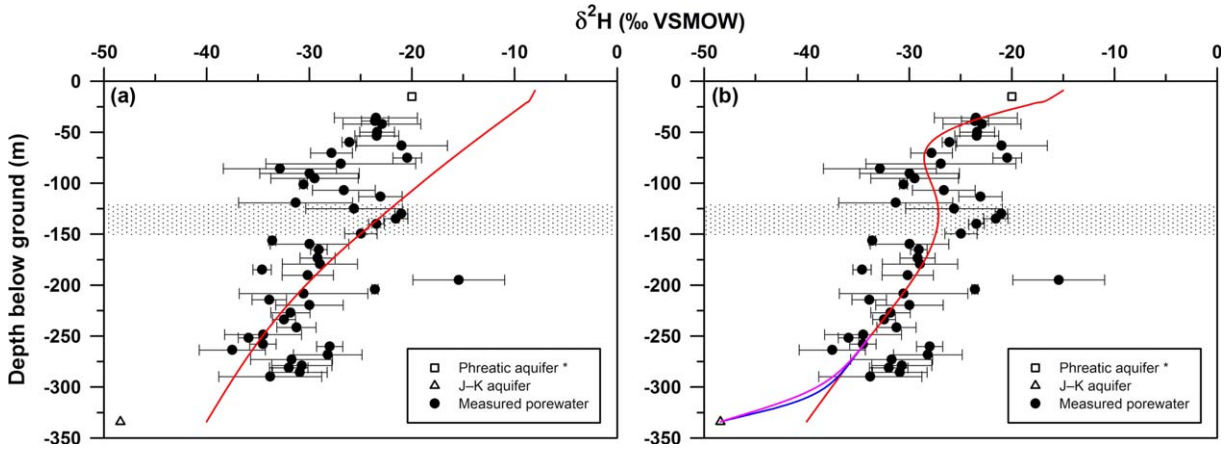

Figure 11. Measured and modeled δ^2H composition of aquitard pore water and confined aquifer at Nancy's Bore. Analytical error for aquifer sample is within the size of the symbol. Composition of phreatic aquifer is estimated, as indicated by the asterisk. Shaded zone corresponds to the location of the Coorikiana Sandstone formation. (a) Measured δ^2H and initial steady state (>4 Ma) simulation (red line). (b) simulated profile after a further 100 ka with a very depleted upper boundary condition, then 20 ka with a more enriched upper boundary condition (red line). The same simulation was repeated with a more depleted lower boundary condition (as measured) after 110 ka (blue line 115 ka; pink line 120 ka).

alternated from depleted (−40‰) to enriched (−30‰) to depleted (−48.4‰) in relatively recent time (cf. Cl^- concentration shifting from fresh to saline). Simulating the net impact of these changes (i.e., −40‰ to −48.4‰) provided inconclusive evidence for the timescale of the changes, although it could be significantly greater than 10 ka (Figure 11b).

4.6. Assumptions and Uncertainty

[68] Uncertainty in the effective diffusion coefficient (D_e) is potentially the greatest source of error in the simulated tracer profiles. Underestimation of D_e causes an overestimation in the time for development of a diffusion profile, and vice versa, but will not affect the ultimate shape of that profile. In the absence of laboratory measurements of D_e on BB2 and NB2 cores, equation (7) was used to estimate D_e from measurements of total porosity ($\mu = 0.40$, $\sigma = 0.06$, $n = 62$; *Gardner et al*. [2012], *Smerdon et al*. [2012]). Thus, uncertainty in D_e lies in the choice of the power term "m." A value of $m = 2.3$ was adopted for the current study based on the average of what were deemed appropriate values in the literature; however, this likely has an error of about ±10%, which would translate to an error of approximately ±20% in the value of D_e.

[69] Understanding how this uncertainty in D_e translates to uncertainty in the simulation time of each profile can be achieved through rearrangement of the well-known expression for characteristic diffusion length:

$$t = \frac{z^2}{4D_e}, \tag{11}$$

where t is the time required for diffusion to account for the majority (about 84%) of concentration change at distance z from the boundary at which the concentration change was applied. It is clear from this equation that a 20% error in D_e results in a 17–25% error in the simulation time. We believe this uncertainty is comparable to that associated with the fixed concentration boundary conditions.

5. Summary and Conclusions

5.1. Evidence of Palaeohydrology

[70] The observed pore water Cl^- profile and, to a lesser degree, δ^2H profile from NB2 revealed important insights to the palaeohydrology of the region during the late Pleistocene and Holocene. The observed Cl^- profile was simulated by implementing three significant palaeohydrological phases: a long-term dry phase until ~120 ka BP, followed by a much wetter (low Cl^- loading) phase from 120 ka to 20 ka BP, and finally a dry (high Cl^- loading) phase from 20 ka BP to present. These periods are broadly consistent with the results of previous studies of Lake Eyre palaeohydrology (e.g., see *Magee et al*., [2004]).

[71] The observed pore water Cl^- profile at BB2 is vastly different to that at NB2. Simulations indicate that considerable deposition of wind-blown salt has occurred at this site for the last ~60 ka. The salt is presumably leached to the shallow water table following episodic rain events, after which the groundwater salinity increases by evaporative discharge and Cl^- is lost into the aquitard via downward diffusion. Further support for the shallow, phreatic aquifer being a discharge zone is provided by the presence of gypsum crystals in the shallow soil crust, as well as the measured carbon-14 activity for the shallow piezometer at this site (4.0 pmC, Table 1). Usually, it is expected that groundwater in a shallow phreatic aquifer with a water table at ~3.5 m depth would have a "modern" age reflecting recent recharge events. However, the measured carbon-14 activity in the phreatic aquifer at BB2 corresponds to an apparent, uncorrected groundwater age of ~25 ka, indicating this is a net discharge zone.

[72] Differences in the inferred palaeohydrology at Birthday Bore and Nancy's Bore can be explained by their vastly different geomorphological settings, even though they are located only ~26 km apart. The existing groundwater well and the new core hole at NB2 are situated atop a local topographic high, covered in gibber rocks with negligible vegetation, and more than several hundred metres away from a small, ephemeral creek. In contrast, BB2 is located on the edge of a wide floodplain for a large ephemeral river, with abundant grasses and small bushes, and beneath a 20 m-high escarpment. Thus, the two sites have very different surface drainage and groundwater flow systems for the shallow, phreatic aquifer.

[73] By comparing measured Cl^- and δ^2H values from the J-K aquifer with the measured values in the lower half of the aquitard at each site, it is clear that the confined aquifer was fresher (lower Cl^-) and more enriched (higher δ^2H) in the past, reflecting different recharge mechanisms to those occurring currently. Numerical model simulations and measured carbon-14 activities for the confined aquifer (Table 1) indicate the change to current recharge conditions has likely occurred within the last 10 ka to 20 ka. These findings are consistent with the suggestion by *Bröder et al*. [2011] that the climate on the western margin of the GAB was more humid in the last 10–30 ka.

5.2. Estimation of Diffuse Discharge

[74] The adopted value of K_v for the two profiles (1×10^{-13} m s^{-1}) allows estimates to be made of the vertical discharge rate from the J-K aquifer. When multiplied by the current head gradients (0.117 and 0.150), this value of K_v equates a Darcy flux of 3.6 mm per 10,000 years for NB2 and 4.6 mm per 10,000 years for BB2. We propose that these results represent the lowermost limit of discharge flux, whereas previous studies have provided uppermost limits [*Woods et al*., 1990*; Costello et al*., 2008].

5.3. Tracers in Aquitards

[75] Previous literature from thick aquitards in North America and Europe has demonstrated the worth of environmental tracer profiles, particularly Cl^- and δ^2H, as archives of palaeoclimate and past geological conditions. In all of these studies, the greatest signals in the tracer data have resulted from glaciation and the associated decrease in Cl^- concentration and depletion in δ^2H composition from these events. In the current study, we have shown that these tracers, particularly Cl^-, are equally useful for understanding palaeohydrological conditions in arid zones that have not been subjected to glaciation for hundreds of millions of years.

5.4. Conclusion

[76] Continuous vertical profiles of aquitard pore water chloride concentration and stable H/O isotope composition, which were collected from two sites in the western discharge zone of the GAB, reveal a complex history of hydrological conditions and associated salinity regimes in central Australia. Chloride profiles in particular reveal long-term shifts in the salinity—and by inference the near-surface hydrology—of the shallow phreatic aquifer that overlies the GAB throughout the late Pleistocene and Holocene. Numerical simulation of the evolution of these profiles required a bulk vertical hydraulic conductivity for the aquitard of $<1 \times 10^{-12}$ m s^{-1}, which in-turn provided the first real estimates of diffuse leakage rates from this part of the GAB being on the order of several millimetres per ten thousand years. Finally, comparisons between the chemical and isotopic composition of aquitard pore water with those measured in groundwater from the underlying J-K aquifer reveal that the latter has been actively recharged within the last 20–30 ka.

[77] **Acknowledgments.** The authors are extremely grateful for the support provided by landowners and managers of pastoral leases on which drilling and groundwater sampling was undertaken, especially Norm Sims of Anna Creek Station. We also acknowledge the traditional owners of this land, the Arabunna people, from whom project support and heritage site clearance was obtained prior to drilling. Field assistance at the time of drilling was enthusiastically provided by Virginia Chostner (University of Saskatchewan), Amanda Treijs, Stacey Priestly and Andrew Love (Flinders University of South Australia), and Daniel Wohling (SA Department for Water). Permission to sample existing shallow, regional bores was kindly provided by Blair Douglas and Murray Tyler of BHP Billiton Pty Ltd., and by Justin Costello of the University of Melbourne. Funding for this work was provided in part through the Australian Government National Water Commission's Groundwater Action Plan, administered through the South Australian Arid Lands Natural Resources Management Board and Flinders University, and in part by CSIRO Water for a Healthy Country National Research Flagship. Hendry received funding through an NSERC Research Chair. Finally, the authors wish to thank Andrew Taylor for assistance in drafting figures and Axel Suckow, Andrew Herczeg and three anonymous reviewers for useful comments on earlier versions of this manuscript.

References

American Society for Testing and Materials (ASTM) (2009) D7263–09: Standard Test Methods for Laboratory Determination of Density (Unit Weight) of Soil Specimens. In: Annual Book of ASTM Standards, West Conshohocken, PA.

American Society for Testing and Materials (ASTM) (2010) D2216–10: Standard Test Methods for Specific Gravity of Soil Solids by Water Pycnometer. In: Annual Book of ASTM Standards, West Conshohocken, PA.

Barbour, S. L., M. J. Hendry, and L. I. Wassenaar (2012), In situ experiment to determine advective-diffusive controls on solute transport in a clay-rich aquitard, *J. Contam. Hydrol.*, *131*(1–4), 79–88.

Bentley, H. W., F. M. Phillips, S. N. Davis, M. A. Habermehl, P. L. Airey, G. E. Calf, E. Elmore, H. E. Gove, and T. Torgersen (1986), Chlorine 36 dating of very old groundwater 1. The Great Artesian Basin, *Australia, Water Resour. Res.*, *22*, 1991–2001.

Bethke, C. M., X. Zhao, and T. Torgerson (1999), Groundwater flow and the 4He distribution in the Great Artesian Basin of Australia, *J. Geophys. Res.*, *104*(B6), 12999–13011.

Birks, S. J., V. H. Remenda, and T. W. D. Edwards (2000), Clay aquitards as isotopic archives of Holocene palaeoclimate in the North Great Plains: sensitivity analysis, *Hydrol. Process.*, *14*, 1523–1536.

Boving, T. B., and P. Grathwohl (2001), Tracer diffusion coefficients in sedimentary rocks: correlation to porosity and hydraulic conductivity, *J. Contam. Hydrol.*, *53*, 85–100.

Bowler, J. M. (1978), Glacial age aeolian events at high and low latitudes: A southern hemisphere perspective, in *Antarctic Glacial History and World Palaeoenvironments*, edited by E. M. van Zinderen Bakker, pp. 149–172, Balkema, Rotterdam.

Bröder, L., R. Purtschert, A. Love, S. Fulton, D. Wohling, and W. Aeschbach-Hertig (2011), Palaeoclimate record from groundwater of the Great Artesian Basin, Australia, *Goldschmidt Conf. Abst.*, 2011.

Cendón, D. I., J. R. Larsen, B. G. Jones, G. C. Nanson, D. Ricklema, S. I. Hankin, J. J. Pueyo, and J. Maroulis (2010), Freshwater recharge into a shallow saline groundwater system, Cooper Creek floodplain, Queensland, *Australia, J. Hydrol.*, *392*, 150–163.

Costelloe, J. F., E. C. Irvine, A. W. Western, V. Matic, J. Walker, and M. Tyler (2008), Quantifying near-surface, diffuse groundwater discharge along the south-west margin of the Great Artesian Basin, Water Down Under 2008, Conference Proceedings, pp. 831–840.

Davis, S. N., D. O. Whittemore, and J. Fabryka-Martin (1998), Uses of chloride/bromide ratios in studies of potable water, *Ground Water*, *36*, 338–350. doi: 10.1111/j.1745–6584.1998.tb01099.x.

Desaulniers, D. E., J. A. Cherry, and P. Fritz (1981), Origin, age and movement of pore water in argillaceous Quaternary deposits at four sites in southwestern Ontario, *J. Hydrol.*, *50*, 231–257.

DeVogel, S. B., J. W. Magee, W. F. Manley, and G. H. Miller (2004), A GIS-based reconstruction of late Quaternary palaeohydrology: Lake Eyre, arid central Australia, Palaeogeog. Palaeoclim. *Palaeoecol.*, *204*, 1–13.

Freeze, R. A., and J. A. Cherry (1979), *Groundwater*, Prentice-Hall, New Jersey, 604 pp.

Fetter, C. W. (1993), *Contaminant Hydrogeology*, Macmillan, New York, 458 pp.

Gale, S. J. (1992), Long-term landscape evolution in Australia, *Earth Surf. Process. Landforms*, *17*, 323–343.

Gardner, W. P., G. A. Harrington, and B. D. Smerdon (2012), Using excess 4He to quantify variability in aquitard leakage, *J. Hydrol.*, *468–469*, 63–75.

Grathwohl, P. (1998), *Diffusion in Natural Porous Media: Contaminant Transport, Sorption/Desorption and Dissolution Kinetics*, Kluwer Academic, Boston, 224 pp.

Habermehl, M. A. (1980), The Great Artesian Basin, Australia, Bur. Miner. Resour. J. Aust. Geol. *Geophys.*, *5*, 9–38.

Habermehl, M. A., J. Devonshire, and J. Magee (2009), Sustainable groundwater allocations in the intake beds of the Great Artesian Basin in New South Wales, in Final Report for the National Water Commission, Bureau of Rural Sciences, Canberra.

Habermehl, M. A., and J. E. Lau (1997), Hydrogeology of the Great Artesian Basin (Map at scale 1: 2 500 000), Australian Geological Survey Organisation, Canberra.

Harrington, G. A., M. J. Hendry, and N. I. Robinson (2007), The impact of permeable conduits on solute transport in aquitards: mathematical models and their application, *Water Resour. Res.*, *43*, W05441, doi:10.1029/2005WR004144.

Harrington, G. A., A. J. Love, and A. L. Herczeg (2001), Relative importance of physical and geochemical processes affecting solute distributions in a clay aquitard, in Water-Rock Interaction 2001, edited by Cidu, R., Lisse, the Netherlands, pp. 177–180.

Hendry, M. J., T. G. Kotzer, and D. K. Solomon (2005), Sources of radiogenic helium in a clay till aquitard and its use to evaluate the timing of geologic events, *Geochim. Cosmochim. Acta*, *69*(2), 475–483.

Hendry, M. J., and L. I. Wassenaar (1999), Implications of the distribution of dD in pore waters for groundwater flow and the timing of geologic events in a thick aquitard system, *Water Resour. Res*. *35*(6), 1751–1760, doi:10.1029/1999WR900046.

Hendry, M. J., and L. I. Wassenaar (2000), Controls on the distribution of major ions in pore waters of a thick surficial aquitard, *Water Resour. Res*. *36*(2), 503–513, doi:10.1029/1999WR900310.

Hendry, M. J., L. I. Wassenaar, and T. G. Kotzer (2000), Chloride and chlorine isotopes (36Cl and d37Cl) as tracers of solute migration in a thick, clay-rich aquitard system, *Water Resour. Res.*, *36*(1), 285–296.

Hendry, M. J., and A. D. Woodbury (2007), Clay aquitards as archives of Holocene paleoclimate: d18O and thermal profiling, *Ground Water*, *45*(6), 683–691.

Hendry, M. J., S. L. Barbour, J. Zetti, V. Chostner, and L. I. Wassenaar (2011), Controls on the long-term downward transport of δ2H of water in a regionally extensive, two-layered aquitard system, *Water Resour. Res.*, *47*, W06505, doi:10.1029/2010WR010044.

Ingebritsen, S. E., W. E. Sanford, and C. E. Neuzil (2006), *Groundwater in Geologic Processes*, Cambridge Univ. Press, Cambridge, 536 pp.

Kellett, J. R., T. R. Ransley, J. Coram, J. Jaycock, D. F. Barclay, G. A. McMahon, L. M. Foster, and J. R. Hillier (2003), Groundwater recharge in the Great Artesian Basin intake beds, Queensland, in Final Report for the NHT Project #982713 Sustainable Groundwater Use in the GAB Intake Beds, Queensland, BRS, Natural Resources and Mines, Queensland Government.

Kotwicki, V. (1986), Floods of Lake Eyre, Engineering and Water Supply Department, *South Australia*, 99 pp.

Krieg, G. W. (1995), Mesozoic, in The Geology of South Australia. Vol. *2*: The Phanerozoic, edited by Drexel, J. F., and W. V. Preiss, South Australia Geological Survey, Bulletin 54, pp. 93–150.

Li, Y.-H., and S. Gregory (1974), Diffusion of ions in sea water and in deep-sea sediments, *Geochim. Cosmochim. Acta 38*, 703–714.

Love, A. J., A. L. Herczeg, and G. Walker (1996), Transport of water and solutes across a regional aquitard inferred from porewater deuterium and chloride profiles, Otway Basin, Australia, in Isotopes in Water Resources Management, *Int. At. Energy Agency, Vienna, Austria*, 1996, pp. 273–286.

Love, A. J., A. L. Herczeg, L. Sampson, R. G. Cresswell, and L. K. Fifield (2000), Sources of chloride and implications for 36Cl dating of old groundwater, southwestern Great Artesian Basin, *Australia, Water Resour. Res.*, *36*(6), 1561–1574.

MacDonald, M. G., and A. W. Harbaugh (1996), User's documentation: MODFLOW-96, An update to the USGS Modular three-dimensional finite-difference groundwater flow model, in US Geol. Survey Open File Rept., pp. 96–485.

Magee, J. W., J. M. Bowler, G. H. Miller, and D. L. G. Williams (1995), Stratigraphy, sedimentology, chronology and palaeohydrology of Quaternary lacustrine deposits at Madigan Gulf, Lake Eyre, South Australia, Palaeogeog. *Palaeoclim. Palaeoecol.*, *113*, 3–42.

Magee, J. W., and G. H. Miller (1998), Lake Eyre palaeohydrology from 60 ka to present: beach ridges and glacial maximum aridity, *Palaeogeog. Palaeoclim. Palaeoecol.*, *144*, 307–329.

Magee, J. W., G. H. Miller, N. A. Spooner, and D. Questiaux (2004), Continuous 150 k.y. monsoon record from Lake Eyre, Australia: Insolation-forcing implications and unexpected Holocene failure, *Geology 32*(10), 885–888.

Mazor, E. (1995), Stagnant aquifer concept Part 1. Large-scale artesian systems - Great Artesian Basin, *Australia, J. Hydrol.*, *173*(2), 19–240.

Mazurek, M., P. Alt-Epping, A. Bath, T. Gimmi, N. Waber, S. Buschaert, P. De Canniere, M. De Craen, A. Gautschi, S. Savoye, A. Vinsot, I. Wemaere, and L. Wouters (2011), Natural tracer profiles across argillaceous formations, *Appl. Geochem.*, *26*, 1035–1064.

Mills, R. (1973), Self-diffusion in normal and heavy water in the range 1–45E, *J. Phys. Chem.*, *77*, 685–688.

Moore, P. S., and G. M. Pitt (1985), *Cretaceous subsurface of the southwestern Eromanga Basin: a review*, in Stratigraphy, Palaeontology, Malacology – Papers in Honour of Dr. Nell Ludbrook, edited by Lindsay, J. M., South Australia Department of Mines and Energy, Special Publication 5, pp. 269–286.

Neuzil, C. E. (1993), Low fluid pressure within the Pierre Shale: a transient response to erosion, *Water Resour. Res.*, *29*(7), 2007–2020.

Novakowski, K. S., and G. van der Kamp (1996), The radial diffusion method: 2. A semianalytical model for the determination of effective diffusion coefficients, porosity, and adsorption, *Water Resour. Res.*, *32*(6), 1823–1830. doi:10.1029/95WR03720.

Osenbrück, K., J. Lippmann, and C. Sonntag (1998), Dating very old pore waters in impermeable rocks by noble gas isotopes, *Geochim. Cosmochim. Acta*, *62*(18), 3041–3045.

Sanford, W. E., and W. W. Wood (1995), Paleohydrologic record from lake brine on the southern High Plains, *Texas. Geol.*, *23*(3), 229–232.

Singh, G. (1981), Late Quaternary pollen records and seasonal palaeoclimates of Lake Frome, South Australia, *Hydrobiologia*, *82*, 419–430.

Smerdon, B. D., G. A. Harrington, W. P. Gardner, and L. Smith (2012), Using in-situ pore pressure to constrain the permeability of a major confining layer in the Great Artesian Basin. International Association of Hydrogeologist 2012 Congress, Niagara Falls, Canada. https://publications.csiro.au/rpr/pub?pid=csiro:EP121765.

Torgersen, T., and W. B. Clarke (1985), Helium accumulation in groundwater, I: An evaluation of sources and the continental flux of crustal 4He in the Great Artesian Basin, Australia, Geochim. *Cosmochim. Acta*, *49*, 1211–1218.

Tweed, S., M. Leblanc, I. Catrwright, G. Favreau, and C. Leduc (2011), Arid zone groundwater recharge and salinisation processes; an example from the Lake Eyre Basin, *Australia, J. Hydrol.*, *408*, 257–275.

Ullman, W. J., and L. C. McLeod (1986), The late-Quaternary salinity record of Lake Frome, South Australia: evidence from Na+ in stratigraphically preserved gypsum, Palaeogeog. Palaeoclim. *Palaeoecol.*, *54*, 153–169.

Van Loon, L. R., W. Muller, and K. Iijima (2005), Activation energies of the self-diffusion of HTO, 22Na+ and 36Cl− in a highly compacted argillaceous rock (Opalinus Clay), *Appl. Geochem.*, *20*, 961–972.

Van Loon, L. R., M. A. Glaus, and W. Muller (2007), Anion exclusion effects in compacted bentonites: Towards a better understanding of anion diffusion, *Appl. Geochem.*, *22*, 2536–2552.

Wassenaar, L. I., and M. J. Hendry (2000), Mechanisms controlling the distribution and transport of 14C in a clay-rich till aquitard, *Ground Water*, *38*(3), 343–349.

Wassenaar, L. I., M. J. Hendry, V. L. Chostner, and G. P. Lis (2008), High resolution pore water d2H and d18O measurements by H2O(liquid)-H2O(vapour) equilibration laser spectroscopy, *Environ. Sci. Technol.*, *42*, 9262–9267.

White, D. C., and M. M. Lewis (2011), A new approach to monitoring spatial distribution and dynamics of wetlands and associated flows of

Australian Great Artesian Basin springs using QuickBird satellite imagery, *J. Hydrol.*, *408*, 140–152.

Williams, A. F., and J. W. Holmes (1978), A novel method of estimating the discharge of water from mound springs of the Great Artesian Basin, *central Australia, J. Hydrol.*, *38*(3–4), 263–272, doi:10.1016/0022–1694(78)90073-2.

Wood, W. W., and W. E. Sanford (1995), Eolian transport, saline lake basins, and groundwater solutes, *Water Resour. Res.*, *31*(12), 3121–3129.

Wood, W. W., and W. E. Sanford (2007), Atmospheric bromine flux from the coastal Abu Dhabi sabkhat: A ground-water mass-balance investigation, *Geophys. Res. Lett.*, *34*, 14.

Woods, P. H., G. R. Walker, and G. B. Allison (1990), Estimating groundwater discharge at the southern margin of the Great Artesian Basin near Lake Eyre, South Australia, in Proceedings of International Conference on Groundwater in Large Sedimentary Basins, Perth, Australia, 1990, pp. 298–309.

Yang, Y., and A. C. Aplin (2010), A permeability-porosity relationship for mudstones, *Marine Petrol. Geol.*, *27*, 1692–1697.

Zheng, C., and G. D. Bennett (1995), *Applied Contaminant Transport Modelling: Theory and Practice*, Wiley, New York.

Zheng, C., and P. P. Wang (1999), MT3DMS: A modular three-dimensional multispecies transport model from simulation of advection, dispersion, and chemical reactions of contaminants in groundwater systems; documentation and user's guide, US Army Corps of Engineers, Contract Report SERDP-99-1, December 1999.